Journal of Solid State Chemistry 245 (2017) 61–66

Contents lists available at ScienceDirect

Journal of Solid State Chemistry

journal homepage: www.elsevier.com/locate/jssc

Synthesis and magnetic structure of the layered manganese oxide selenide $Sr_2MnO_2Ag_{1.5}Se_2$

Jack N. Blandy[a,b], Jelena C. Boskovic[a], Simon J. Clarke[a,*]

[a] Department of Chemistry, University of Oxford, Inorganic Chemistry Laboratory, South Parks Road, Oxford OX1 3QR, United Kingdom
[b] Diamond Light Source Ltd., Harwell Science and Innovation Campus, Didcot OX11 0DE, United Kingdom

ARTICLE INFO

Keywords:
Oxychalcogenide
Oxide selenide
Magnetic order
A-type magnetic structure

ABSTRACT

The synthesis of a high-purity sample of the layered oxide selenide $Sr_2MnO_2Ag_{1.5}Se_2$ is reported. At ambient temperature it crystallises in the space group $I4/mmm$ with two formula units in the unit cell and lattice parameters a=4.08771(1) Å, c=19.13087(8) Å. The compound displays mixed-valent manganese in a formal oxidation state close to +2.5 and powder neutron diffraction measurements reveal that below the Néel temperature of 63(1) K this results in an antiferromagnetic structure which may be described as A-type, modelled in the magnetic space group P_I4/mnc (128.410 in the Belov, Neronova and Smirnova (BNS) scheme) in which localised Mn moments of 3.99(2) μ_B are arranged in ferromagnetic layers which are coupled antiferromagnetically. In contrast to the isostructural compound $Sr_2MnO_2Cu_{1.5}S_2$, $Sr_2MnO_2Ag_{1.5}Se_2$ does not display long range ordering of coinage metal ions and vacancies, nor may significant amounts of the coinage metal readily be deintercalated using soft chemical methods.

1. Introduction

Oxide chalcogenides of composition $A_2MO_2X_2Ch_2$ (A=Sr, Ba; M=1st row transition metal or Zn, X=Cu, Ag and Ch=S, Se) were first discovered by Zhu and Hor in 1997 [1,2]. The crystal structure, shown in Fig. 1, is similar to that originally described for $Sr_2Mn_3Sb_2O_2$ [3]. The transition metal, M, is in an unusual coordination environment in which it is in a square-planar coordination by oxide ions, forming MO_2 sheets, and in which it is additionally coordinated by two axial chalcogenide ions which complete a distended MO_4Ch_2 octahedron [4]. We have previously shown [5] that the compound originally reported as $Sr_2MnO_2Cu_2S_2$ [2] is in fact highly copper deficient in the chalcogenide layers and the composition accessible in a high temperature synthesis is $Sr_2MnO_2Cu_{1.5}S_2$. In this compound and in the selenide analogue $Sr_2MnO_2Cu_{1.5}Se_2$ [5,6] the Cu deficiency (25% of the Cu sites are vacant) means that the average oxidation state of Mn is approximately +2.5. These two compounds with Cu^+ in tetrahedral coordination by sulfide or by selenide behave quite differently at low temperatures. The Cu vacancies order crystallographically below ~250 K in $Sr_2MnO_2Cu_{1.5}S_2$ resulting in strong superstructure reflections. In contrast, in $Sr_2MnO_2Cu_{1.5}Se_2$ no additional Bragg peaks appear in the powder X-ray diffraction (PXRD) pattern at low temperatures, although some evidence for short-range ordering appears in electron diffraction patterns [6]. We have previously described how the length scale of the Cu/vacancy ordering evolves in the solid solution $Sr_2MnO_2Cu_{1.5}(Se_{1-x}Se_x)_2$ [6]. The absence of long-range vacancy ordering in the selenide-rich compounds may be because there is less of a thermodynamic driving for ordering, or the Cu ion mobility is slightly lower than in the sulfide analogue [6].

In both $Sr_2MnO_2Cu_{1.5}S_2$ and $Sr_2MnO_2Cu_{1.5}Se_2$ the localised Mn moments show long range magnetic order, but the magnetic structures are very different. In both compounds, the mixed valence results in strong ferromagnetic coupling between moments within the MnO_2 sheets, but in the sulfide case the magnetic structure consists of ferromagnetic zig-zag chains within the sheets, which are coupled antiferromagnetically (the so-called CE type structure), while in the selenide case each sheet displays ferromagnetic coupling and the planes are coupled antiferromagnetically (the so-called A-type structure) [6]. This magnetic structure is also adopted by related compounds with thicker copper sulfide layers [5]. Thus in these mixed-valent manganese compounds where the oxidation states are between +2 and +3, similar competition exists as is found in mixed-valent manganese oxides with mean oxidation states similar to +3.5 [7–10]. Adamson et al. [6] suggested a correlation exists between the shortening length scale of the coinage metal/vacancy ordering and the tendency of A-type magnetic ordering to be adopted (as opposed to the CE-type), however this requires further investigation.

$Sr_2MnO_2Cu_{1.5}S_2$ and $Sr_2MnO_2Cu_{1.5}Se_2$ also exhibit differences in

* Corresponding author.
E-mail address: simon.clarke@chem.ox.ac.uk (S.J. Clarke).

http://dx.doi.org/10.1016/j.jssc.2016.10.010
Received 18 August 2016; Received in revised form 4 October 2016; Accepted 10 October 2016
Available online 11 October 2016

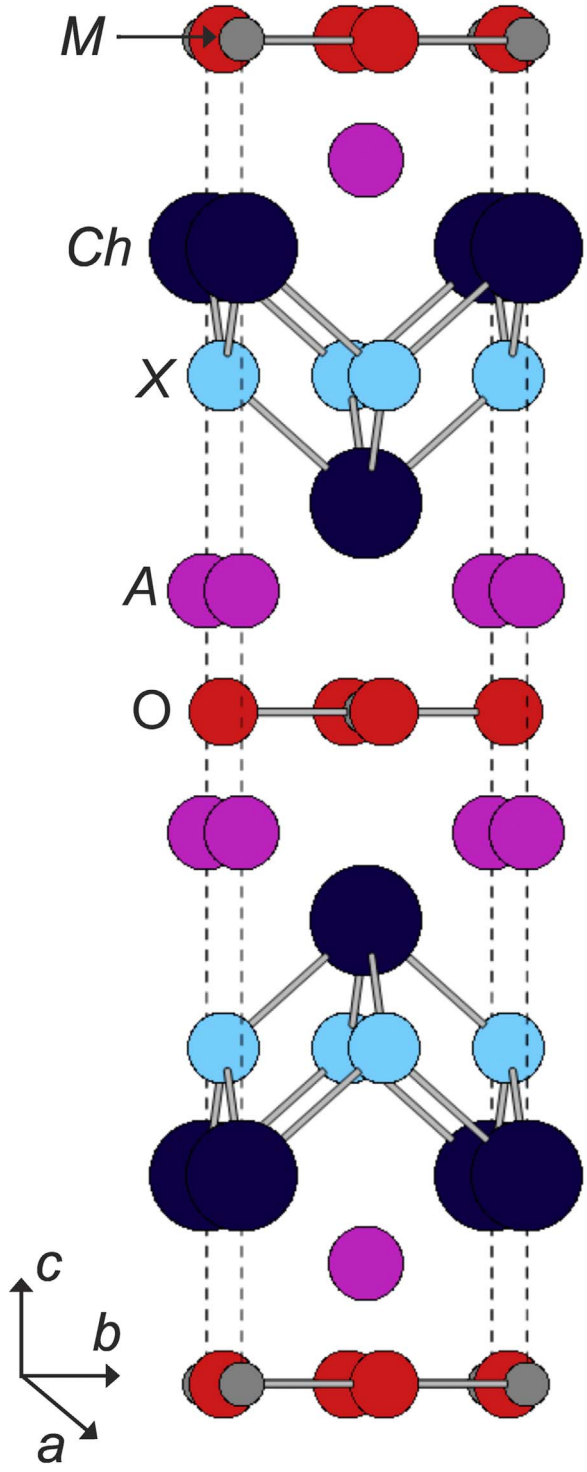

Fig. 1. The crystal structure of $A_2MO_2X_2Ch_2$ (A=Sr, Ba), M=1st row transition metal, X=coinage metal (Cu or Ag), Ch=chalcogenide).

their chemical reactivities. In $Sr_2MnO_2Cu_{1.5}S_2$, Mn may be oxidised topotactically by suspending the compound in a solution of I_2 and acetonitrile. Removal of about 10% of the Cu, resulting in a limiting composition of $Sr_2MnO_2Cu_{1.33}S_2$, leads to the compound adopting an incommensurately-modulated Cu/vacancy ordering scheme at room temperature and the oxidation of Mn results in dramatic changes in the magnetic ordering [11]. In contrast, $Sr_2MnO_2Cu_{1.5}Se_2$ does not appear to be susceptible to deintercalation of Cu by stirring in I_2, a possible reason for this is that the Cu^+ ions are less mobile in the selenide layers.

Jin et al. reported the synthesis of $Sr_2MnO_2Ag_{1.5}Se_2$, [12] having found that the compound formed with an intrinsic Ag deficiency of 0.5 per formula unit compared with the idealised stoichiometric composition "$Sr_2MnO_2Ag_2Se_2$" which would have all sites fully occupied. Magnetometry data suggested that the compound was antiferromagnetically ordered below 67 K. However, it was found that $Sr_2MnO_2Ag_{1.5}Se_2$ could only be synthesised approximately 90 wt% pure via a purely solid-state route [12]. In this work we verify the difficulties in achieving high purity material using purely solid state synthesis techniques, but we report that an I_2 purification step results in the isolation of $Sr_2MnO_2Ag_{1.5}Se_2$, with ~99 wt% purity. This has enabled us to compare and contrast the crystal structure, magnetic ordering and chemical properties with those of the Cu-containing chalcogenide analogues using synchrotron powder X-ray diffraction (PXRD) and powder neutron diffraction (PND).

2. Experimental

2.1. Synthesis

All manipulations were performed in a Glovebox technology Ltd Ar-filled glovebox. $Sr_2MnO_2Ag_{1.5}Se_2$ was synthesised on the 3 g scale from SrO (prepared by thermal decomposition of $SrCO_3$ (Alfa 99.99%)), Mn (Aldrich 99%), Ag (Aldrich 99.9%) and Se (Alfa 99.999%) in the ratio 2:1:2:2. These reactants were thoroughly ground together in an agate pestle and mortar, pressed into 13 mm diameter pellets at a force of 5 t, loaded into an alumina crucible and sealed in silica ampoules under dynamic vacuum. The ampoules were heated to 700 °C at a rate of 10 °C min^{-1} and held at this temperature for 21 days, before being cooled to room temperature. A long heating period was used because it was found that highest sample purities were achieved when comparatively low temperatures and long reaction times were used. The resulting product was tested for purity by laboratory powder X-ray diffraction (PXRD). The purity of the sample was significantly less than when the reaction was performed on a 1 g scale, so the sample was reground and reheated at 700 °C for 3 days. PXRD analysis showed this improved the purity of the sample to approximately 93 wt%, with SrSe and Ag as the dominant impurities.

The sample was then purified by stirring 2.5 g of sample in a solution containing I_2 (0.9979 g, 1.0 M equivalent) and NaI (1.1786 g, 2.0 M equivalents) dissolved in dry acetonitrile, in an ice-bath, under a N_2 atmosphere (using Schlenk line techniques). The suspension was left stirring for two days before removing the solution by filtration. The powder was then washed with dry acetonitrile and dried under vacuum. 2.0 g of powder was isolated by filtration and this appeared phase-pure by laboratory PXRD analysis. I_2 was used to purify the sample because it has been found with similar samples that I_2 removes both SrSe and Ag from the sample. NaI was used in the reaction to increase the solubility of AgI. NaI dissolves readily in acetonitrile, producing an excess of I^- ions in the solution, these react with AgI to form complexes, such as $[AgI_2]^-$, which have a far greater solubility than AgI [13]. This iodine treatment also enabled us to assess whether significant oxidative deintercalation of Ag was possible using this method as has been described for $Sr_2MnO_2Cu_{1.5}S_2$ [11].

2.2. Diffraction measurements

Initial structural characterisation was carried out by powder X-ray diffraction using a PANanlytical Empyrean instrument operating in Bragg-Brentano geometry with a Ge(111) monochromator to select $CuK\alpha_1$ radiation. Detailed structural characterisation was undertaken on the high-resolution synchrotron X-ray powder diffractometer I11 at the Diamond Light Source, UK [14]. Low-temperature PND measurements to probe the crystal structure and to characterise magnetic long range order were performed on the WISH time-of-flight diffractometer at the ISIS Pulsed Neutron Source, UK, which is particularly optimised for long *d*-spacing data for measurement of magnetic ordering [15].

On I11 two batches of a single $Sr_2MnO_2Ag_{1.5}Se_2$ sample, isolated before and after the I_2 purification step, were ground with amorphous boron (to reduce preferred orientation and absorption effects), loaded in 0.5 mm diameter borosilicate glass capillaries and measured at room temperature using Si-calibrated X-rays, with wavelength of approximately 0.826 Å (the exact wavelength used for each measurement is given with the Rietveld plots). Data were collected in the range $2 \leq 2\theta/° \leq 92$ using the Mythen position-sensitive detector (PSD) and in the range $0 \leq 2\theta/° \leq 150$ using the Multi-Analyser-Crystal (MAC) detector.

Low-temperature PND measurements were performed on WISH using a multi-wavelength beam of neutrons on the same sample purified using I_2 that had been used for the PXRD measurements. This sample (1.9 g in mass) was loaded in to a 6 mm diameter cylindrical vanadium sample can. Data were collected at 1.7, 55, 60, 65, 70 and 125 K inside an Oxford Instruments cryostat. Rietveld refinement against both PND and PXRD data were conducted using the TOPAS Academic Version 5 software [16]. The magnetic structure was determined using ISODISTORT [17] in conjunction with TOPAS Academic.

2.3. Magnetometry

The magnetic properties of the sample were measured on a Quantum Design MPMS-XL SQUID magnetometer. 15–20 mg batches of powder were contained in gelatin capsules. Temperature dependent measurements in the range $2 \leq T/K \leq 300$ were carried out on warming in an applied magnetic field of 100 Oe either after cooling in zero applied field (zero-field-cooled (ZFC)) or after cooling in the measuring field (Field-cooled (FC)). Additional measurements in the range $150 \leq T/K \leq 300$, made at applied fields of 30 kOe and 40 kOe, were used to obtain the intrinsic high temperature magnetic susceptibility because magnetisation isotherms (see Appendix A, Fig. S4) revealed a very slight deviation from linearity at low fields which may be due to a minuscule amount of a magnetic impurity (estimated as < 0.006 wt% of adventitious elemental iron). Magnetisation isotherms were measured in the field range $-50 \leq H/kOe \leq +50$.

3. Results and discussion

3.1. Crystal structure

Synchrotron PXRD measurements were used to probe any changes in the structure of the compound during the purification step using I_2. Stirring in an iodine solution in acetonitrile has been used to deintercalate copper in the related compound $Sr_2MnO_2Cu_{1.5}S_2$, and in that case is accompanied by a contraction of the unit cell volume by 1.6% and the appearance of superstructure reflections [11].

Table 1 compares selected refined parameters of the sample of $Sr_2MnO_2Ag_{1.5}Se_2$ before purification and after purification with the parameters published by Jin et al. [12] The Rietveld refinement against the PXRD data is shown in Fig. 2 for the purified sample and further plots and tables of structural parameters are supplied in the Supplementary Material (Appendix A: Figs. S1 & S2, Tables S1 & S2).

Table 1 shows that the I_2 purification step reduces the unit cell volume by 0.588(6) Å^3 (0.18%), this is significantly larger than the difference in cell volume obtained in two separate measurements on the purified sample measured using the different detectors on I11 (see Table S1; there is ~0.1 Å^3 (~0.03%) apparent difference between the volumes measured using the Mythen PSD and the MAC detector for the purified sample), so may be judged to be the result of a real reduction in Ag occupancy which occurs during the reaction with I_2. In the $Sr_2MnO_2Cu_{1.5}S_2$ system, deintercalation of 11% of the Cu from $Sr_2MnO_2Cu_{1.5}S_2$ results in a 1.6% reduction in cell volume [11]. Extrapolating this trend to $Sr_2MnO_2Ag_{1.5}Se_2$ allows us to estimate that only ~1% of the Ag in $Sr_2MnO_2Ag_{1.5}Se_2$ has been deintercalated in the I_2 purification step, and this is not contradicted by the independent refinement of the Ag site occupancy before and after purification. We note that the cell volume after the purification step is marginally larger than that reported by Jin et al., but the samples were not all measured on the same diffractometer. We conclude that a variation in Ag occupancy of about 1% is accessible using the purification with I_2; we cannot rule out that a similar variation in Ag occupancies is also accessible via a purely solid state synthesis route for this compound.

Data were also recorded independently on I11 using the MAC detector for the sample after purification. The use of the analyser crystals mean that the MAC detector offers higher resolution, more accurate lattice parameters and is less sensitive to anomalies, such as capillary precession, than the Mythen PSD. Fig. 2 shows the Rietveld plot for the purified sample. The refined parameters are given in Tables S1 and S2 (in Appendix A) and Table 2 lists important structural parameters obtained from this refinement. Independent refinements of the Ag site occupancies from the MAC and PSD data sets obtained on I11 produced a mean Ag site occupancy of 0.770(3). Refinement of the structure of the same sample against PND data at 125 K and 1.7 K (see Fig. 6 below and Figs. S5–S10 and Tables S3–S6 in Appendix A) produced an Ag site occupancy of 0.750(4). We deduce that a composition of $Sr_2MnO_2Ag_{1.52(2)}Se_2$ reflects the realistic uncertainty on the refined composition from our PXRD and PND measurements. We note that this large Ag deficiency relative to the idealised "$Sr_2MnO_2Ag_2Se_2$" stoichiometry seems to be intrinsic to samples made at high temperatures [12] because additional Ag than is required by the $Sr_2MnO_2Ag_{1.5}Se_2$ composition remains as a spectator phase during the synthesis and is removed in the purification step.

Selected structural parameters are compared for $Sr_2MnO_2Cu_{1.5}S_2$, $Sr_2MnO_2Cu_{1.5}Se_2$ and $Sr_2MnO_2Ag_{1.5}Se_2$ in Table 2. As the sizes of the coinage metal and chalcogenide ions increase the c/a ratio increases dramatically. This is due to a relatively small increase in a (which is equal to twice the Mn–O bond length), so consequently the c lattice parameter increases disproportionately and expands by ~1.25 Å (~7%) as Cu^+ in $Sr_2MnO_2Cu_{1.5}Se_2$ is replaced by Ag^+ in $Sr_2MnO_2Ag_{1.5}Se_2$. This results in a large distortion of the $AgSe_4$ tetrahedron in $Sr_2MnO_2Ag_{1.5}Se_2$ compared with the almost regular $CuSe_4$ tetrahedron in $Sr_2MnO_2Cu_{1.5}Se_2$, (Fig. 3). Despite repeated attempts, we have been unable to make a sample containing the sulfide analogue phase $Sr_2MnO_2Ag_{1.5}S_2$, presumably because the tetrahedron becomes too distorted and the quinary phase is unstable with respect to the binaries SrS, MnO which are formed along with elemental Ag.

3.2. Magnetometry

Magnetic susceptibility measurements were performed on the sample before and after purification to assess whether the purification step caused a significant change in magnetic behaviour. The magnetic susceptibility measurements (Fig. 4(a)) show that the sample is paramagnetic above 63(1) K, where an antiferromagnetic transition occurs.

Table 1
Refined parameters from Rietveld refinement of the $Sr_2MnO_2Ag_{1.5}Se_2$ samples before and after purification and comparison with data published by Jin et al. [12].

Parameter	Before purification	After purification	Jin et al.
X-ray source	Synchrotron I11[a]	Synchrotron I11[a]	Cu Kα
Wavelength (Å)	0.826222	0.825953	1.5418
Purity by mass (%)	92	~99	90
Space group	*I4/mmm*	*I4/mmm*	*I4/mmm*
a (Å)	4.08973(2)	4.08771(1)	4.0882(1)
c (Å)	19.14709(9)	19.13087(8)	19.1179(2)
V (Å^3)	320.252(3)	319.664(3)	319.525(5)
Ag occupancy	0.7852(7)	0.7733(6)	0.720(2)
ωR_p (%)	1.183	0.854	4.57

[a] Both measured using the same detector (PSD) for comparison, the fits are shown in Figs. S1 and S2.

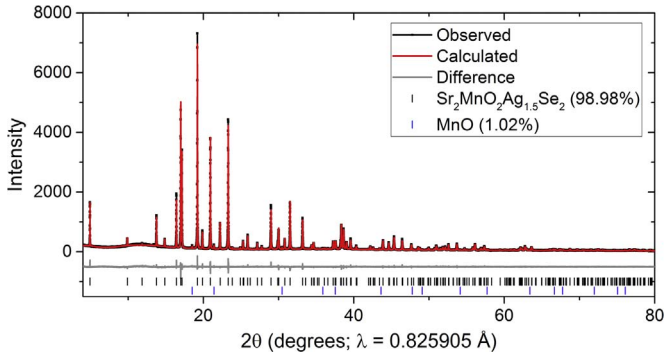

Fig. 2. Rietveld refinement of the purified sample of $Sr_2MnO_2Ag_{1.5}Se_2$, against I11 data (MAC detector) at room temperature (See Tables S1 and S2 and Table 2).

Table 3 compares magnetometry data from the sample described in this paper (before and after purification) with data from Jin et al. [12] The Weiss temperature (θ) and effective magnetic moment (μ_{eff}) were derived from the linear 150–300 K region of the inverse susceptibility (see Fig. 4(b) and S3–S4).

The data show that T_N, θ and μ_{eff} are similar within the experimental uncertainty before and after purification. The calculated μ_{eff} is in between the values that expected from the spin-only formula for high-spin octahedral Mn^{2+}(5.92 μ_B) and Mn^{3+}(4.90 μ_B), this reflects that Mn in the compound has an oxidation state between +2 and +3. Similar values of the effective moment were found for $Sr_2MnO_2Cu_{1.5}S_2$ (5.45(3) μ_B) [5] and $Sr_2MnO_2Cu_{1.5}Se_2$ (5.63(3) μ_B), [6] which are both close analogues of $Sr_2MnO_2Ag_{1.5}Se_2$.

The 100 Oe susceptibility data (Fig. 4(a)) reveal a slight divergence of ZFC and FC data below T_N, similar to that observed in the original report of $Sr_2MnO_2Cu_{1.5}S_2$ [2]. The magnetisation isotherm (Fig. 5), measured at 5 K, is slightly offset from the origin. These observations suggest a small glassy element to the magnetism arising from some disorder and frustration of the magnetic interactions. It is possible that this arises from a slight inhomogeneity in the distribution of Mn^{2+} and Mn^{3+} ions, which itself may arise from the disorder in the distribution of Ag^+ ions and Ag-site vacancies in the compound. The magnetisation isotherm at 5 K (Fig. 5) also shows a slight upwards curvature in the magnetisation at high fields which is not evident in measurements of magnetisation against applied field above the antiferromagnetic ordering temperature (Fig. S4); this suggests that the compound is metamagnetic but that the field-induced antiferromagnetic to ferromagnetic transition would occur at much higher fields than 50 kOe. Metamagnetic behaviour has been observed in the series $Sr_2MnO_2Cu_{2m-\delta}S_{m+1}$, ($m$=2, 3) [5] which have a larger separation between MnO_2 layers. In those compounds the magnetic moments in the MnO_2 layers are coupled ferromagnetically, and the layers are coupled antiferromagnetically in low applied fields. The applied field required to drive the systems into the ferromagnetic state decreases as the separation of the layers increases [5].

3.3. Magnetic structure

Simultaneous refinements against four banks (2/9, 3/8, 4/7 and 5/6) of WISH data at 125 K (Fig. 6(a) and Tables S3 and S4) are in agreement with the structural model derived from PXRD analysis. No additional peaks from long range ordering of Ag^+ ions and vacancies were apparent. The reflection at d=5.07 Å is indexed as the dominant magnetic reflection of MnO (< 1% by mass) [18]. At 1.7 K additional reflections (see Fig. 6(b) and Tables S5 and S6) were evident, which diminished in intensity on warming and vanished above T_N (Fig. S11 and S12). These reflections were indexed on the nuclear unit cell (propagation vector $\boldsymbol{k}$=(0 0 0)), but with a breaking of symmetry, so that the magnetism may be described by space group P_I4/mnc (128.410) in the Belov, Neronova and Smirnova (BNS) scheme; a setting of space group $I_P4/mm'm'$ (139.15.1193) in the Opechowski and Guccione (OG) scheme) [19]. This relaxation of symmetry allows for refinement of the mM3+(a) mode on the Mn sites, which corresponds to A-type antiferromagnetic order, in which the spins are aligned parallel within the MnO_2 planes, but anti-parallel in adjacent MnO_2 planes (see Fig. 6 inset). This model accounts for all additional intensity in the data ($_{\omega}R_P$=3.674%) and gives a refined ordered magnetic moment of 3.99(2) μ_B.

The magnetic structure adopted by $Sr_2MnO_2Ag_{1.5}Se_2$ is similar to that found for $Sr_2MnO_2Cu_{1.5}Se_2$ [6] and the related sulfides $Sr_2MnO_2Cu_{3.5}S_3$ and $Sr_2MnO_2Cu_{5.5}S_4$ [5]. The ordered magnetic moment of $Sr_2MnO_2Cu_{1.5}Se_2$ at base temperature is 4.1(1) μ_B, [6] it is therefore similar within the experimental uncertainty, to that of $Sr_2MnO_2Ag_{1.5}Se_2$. These two compounds are isostructural, with similar refined coinage metal occupancies, indicative of similar Mn oxidation states (~+2.5). The Mn–O distances differ only by 0.01 Å (0.5%), indicating a similar degree of covalency in the compounds. These factors explain the similar ordered magnetic moments for the two phases. However, the Néel temperature, T_N, for three-dimensional ordering is ~9 K lower in $Sr_2MnO_2Cu_{1.5}Se_2$ (53 K) than in $Sr_2MnO_2Ag_{1.5}Se_2$ (63(1) K). Although the c lattice parameter is significantly larger in $Sr_2MnO_2Ag_{1.5}Se_2$, due to the larger size of the coinage metal ion, the Mn–Se distance in $Sr_2MnO_2Ag_{1.5}Se_2$ is 0.04 Å (1.34%) shorter than in $Sr_2MnO_2Cu_{1.5}Se_2$; this, and the different shape of the coinage metal tetrahedron (Fig. 3) may be the factors which lead to slightly stronger inter-plane exchange constants in $Sr_2MnO_2Ag_{1.5}Se_2$ than in $Sr_2MnO_2Cu_{1.5}Se_2$. Direct measurement of the exchange constants using neutron spectroscopy would enable this difference to be investigated in greater detail.

Table 2
Comparison of selected structural parameters for $Sr_2MnO_2Cu_{1.5}S_2$, (PND data from Ref. [5]) $Sr_2MnO_2Cu_{1.5}Se_2$ (PND data from Ref. [6]) and $Sr_2MnO_2Ag_{1.5}Se_2$ (synchrotron PXRD data (Fig. 2)).

	$Sr_2MnO_2Cu_{1.5}S_2$ [5]	$Sr_2MnO_2Cu_{1.5}Se_2$ [6]	$Sr_2MnO_2Ag_{1.5}Se_2$
a (Å)	4.01218(3)	4.06655(3)	4.08798(1)
c (Å)	17.1916(2)	17.8830(1)	19.13391(9)
c/a ratio	4.28485(6)	4.39759(4)	4.68053(3)
V (Å³)	276.743(5)	295.729(5)	319.759(3)
Cu or Ag occupancy	0.745(5)	0.773(2)	0.770(3)
Mn–O distance (Å) [4][a]	2.00608(5)	2.03328(1)	2.04399(1)
Mn–S(Se) distance(Å) [2][a]	2.9200(9)	3.0002(3)	2.9652(5)
Mn–S(Se)/Mn-O ratio	1.4555	1.4779(5)	1.4507(5)
Cu(Ag)–S(Se) distance (Å) [4][a]	2.4337(1)	2.5094(2)	2.7357(3)
S(Se)–Cu(Ag)–S(Se) angle (°) [2][a]	111.03(5)	108.25(5)	96.69(2)
S(Se)–Cu(Ag)–S(Se) angle (°) [4][a]	108.70(5)	110.09(5)	116.215(9)

[a] Numbers in square brackets give the number of bonds/angles of each type. See also Fig. 3.

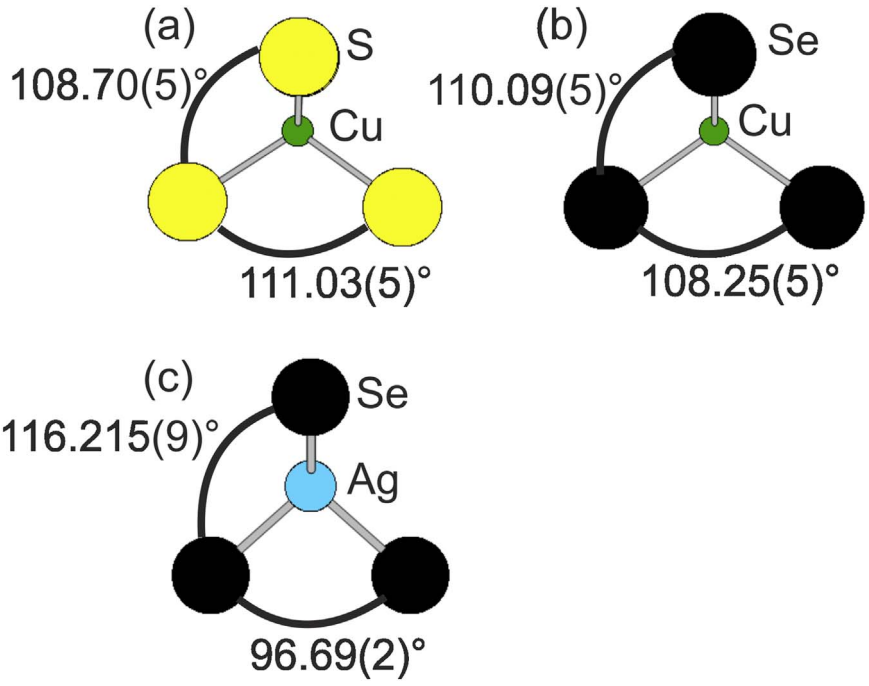

Fig. 3. The $XS(Se)_4$ coordination environment of (a) $Sr_2MnO_2Cu_{1.5}S_2$ [5] and (b) $Sr_2MnO_2Cu_{1.5}Se_2$ [6] and (c) $Sr_2MnO_2Ag_{1.5}Se_2$.

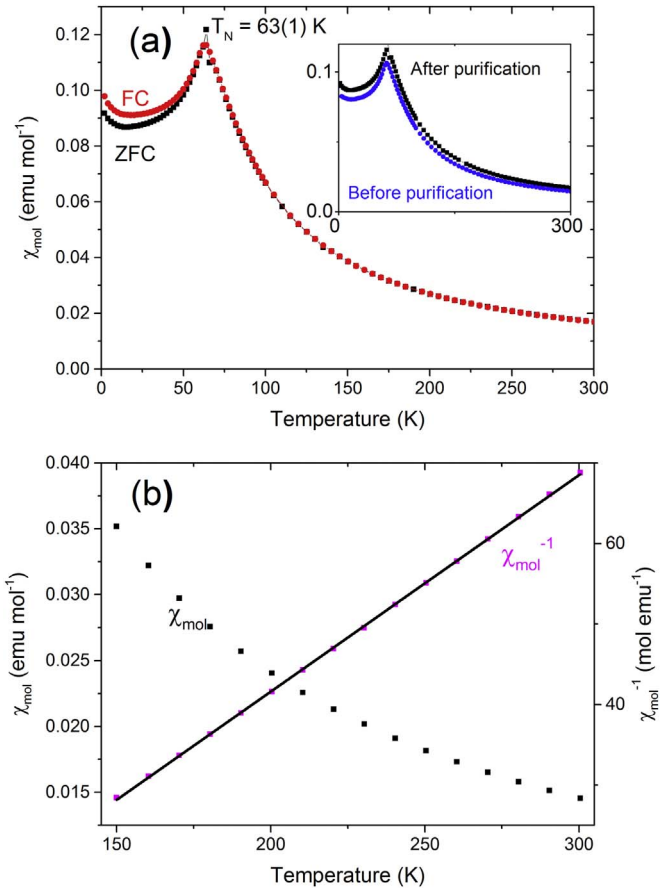

Fig. 4. (a) The magnetic susceptibility of the purified $Sr_2MnO_2Ag_{1.5}Se_2$ sample under ZFC and FC conditions with a measuring field of 100 Oe. The inset compares the ZFC magnetic susceptibility of $Sr_2MnO_2Ag_{1.5}Se_2$ before and after purification. (b) The magnetic susceptibility of the purified sample obtained from measurement in a magnetic field range where the magnetic moment of the sample varies linearly with field (see experimental Section 2.3) and the inverse magnetic susceptibility with line of best fit, from which the effective magnetic moment and Weiss temperature were derived.

Table 3
Comparison of magnetometry data for $Sr_2MnO_2Ag_{1.5}Se_2$ obtained from the samples described in this paper and the sample described by Jin et al. [12].

Parameter	Before purification	After purification	Jin et al.
Néel temperature, T_N (K)	63(1)	63(1)	67
Weiss temperature, θ (K)	+41(2)	+45(3)	+46.8
Effective moment, μ_{eff} (μ_B)	5.47(1)	5.45(1)	5.82(1)

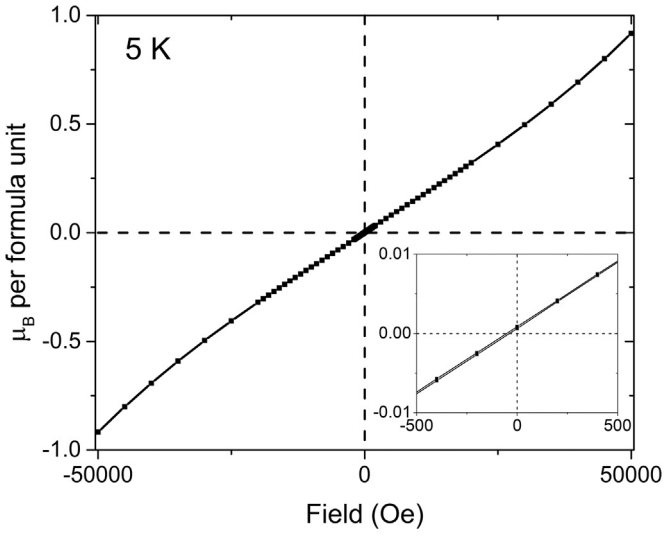

Fig. 5. Magnetisation isotherm of the purified sample of $Sr_2MnO_2Ag_{1.5}Se_2$, measured at 5 K in the range -50 kOe $< H <$ +50 kOe. The inset shows the slight offset from the origin.

4. Conclusions

$Sr_2MnO_2Ag_{1.5}Se_2$ has been synthesised with >99% purity,

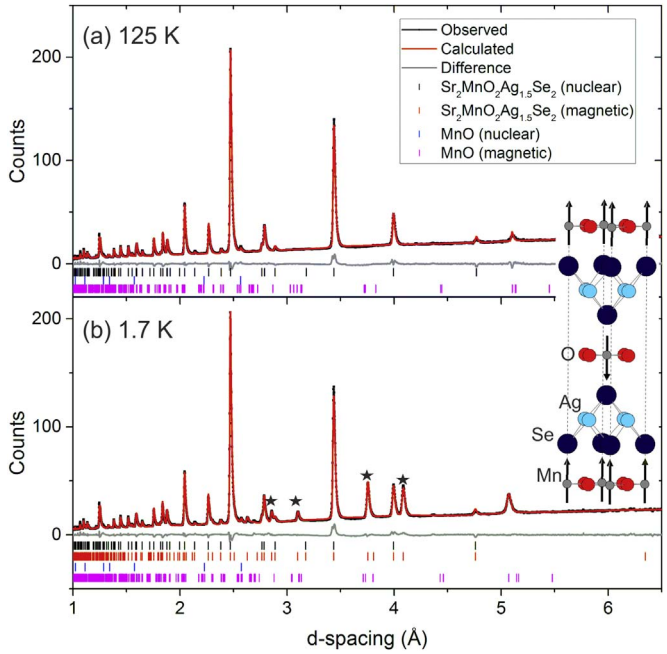

Fig. 6. Rietveld plot of $Sr_2MnO_2Ag_{1.5}Se_2$ measured at (a) 125 K and (b) 1.7 K on the 3/8 (90°) bank of WISH. Stars highlight the four main additional peaks arising from the magnetic structure. The inset shows the magnetic structure, Sr atoms have been omitted for clarity. Plots showing the fits to the other data banks in the Rietveld refinements are supplied in Appendix A.

although an ambient temperature purification step using a solution of I_2 in acetonitrile was required to remove small amounts of impurity phases. This I_2 purification step results in an extremely small (~1%) reduction in Ag occupancy through oxidative deintercalation, showing that only a very narrow phase width is accessible using this soft chemical approach in this case. Magnetic susceptibility measurements in the Curie-Weiss regime produce an effective moment of 5.45(1) μ_B per Mn ion, consistent with the mixed valence (Mn oxidation state of +2.5), and a positive Weiss temperature suggesting that the strongest interactions between Mn moments are ferromagnetic. Below the Néel temperature of 63(1) K the magnetic structure of the compound was accordingly found to be A-type antiferromagnetic (with ferromagnetic coupling of nearest neighbour Mn moments), with a long range ordered moment of 3.99(2) μ_B per Mn ion, similar to that of $Sr_2MnO_2Cu_{1.5}Se_2$ [6]. In $Sr_2MnO_2Ag_{1.5}Se_2$ there is no evidence for a superstructure arising from long range crystallographic ordering of coinage metal ions and vacancies, nor is the coinage metal readily extracted by reaction with iodine. This behaviour is similar to the case of $Sr_2MnO_2Cu_{1.5}Se_2$, but contrasts with the case of $Sr_2MnO_2Cu_{1.5}S_2$ where there is long range Cu/vacancy order and several percent of the Cu ions may readily be extracted by oxidative deintercalation [11]. The coinage ion mobilities [20] and the distribution of the ions [21] in antifluorite-type $Cu_{2-x}S$ and $Cu_{2-x}Se$ ($0 \le x \le 0.2$) are reportedly similar. The different behaviours of the oxide sulfide $Sr_2MnO_2Cu_{1.5}S_2$, and the oxide selenides $Sr_2MnO_2Cu_{1.5}Se_2$ and $Sr_2MnO_2Ag_{1.5}Se_2$ with antifluorite-type coinage metal chalcogenide layers are presumably due to small differences in the thermodynamic driving force for cation/vacancy order or cation deintercalation, and to small differences in ionic mobility.

Acknowledgements

We thank: the UK EPSRC for funding (EP/M020517/1) and for studentship support; the ISIS pulsed neutron and muon source and the Diamond Light Source Ltd (EE13284) for the award of beam time; Diamond for studentship support for JNB; Dr. P Manuel for support on WISH and Dr A Baker and Dr C Murray for support on I11.

Appendix A. Supplementary material

Supplementary data associated with this article can be found in the online version at doi:10.1016/j.jssc.2016.10.010.

References

[1] W.J. Zhu, P.H. Hor, A.J. Jacobson, G. Crisci, T.A. Albright, S.H. Wang, T. Vogt, J. Am. Chem. Soc. 119 (1997) 12398–12399.
[2] W.J. Zhu, P.H. Hor, J. Solid State Chem. 130 (1997) 319–321.
[3] E. Brechtel, G. Cordier, H. Schafer, Z. für Nat. Sect. B J. Chem. Sci. 34 (1979) 777–780.
[4] S.J. Clarke, P. Adamson, S.J.C. Herkelrath, O.J. Rutt, D.R. Parker, M.J. Pitcher, C.F. Smura, Inorg. Chem. 47 (2008) 8473–8486.
[5] Z.A. Gál, O.J. Rutt, C.F. Smura, T.P. Overton, N. Barrier, S.J. Clarke, J. Hadermann, J. Am. Chem. Soc. 128 (2006) 8530–8540.
[6] P. Adamson, J. Hadermann, C.F. Smura, O.J. Rutt, G. Hyett, D.G. Free, S.J. Clarke, Chem. Mater. 24 (2012) 2802–2816.
[7] D.N. Argyriou, H.N. Bordallo, B.J. Campbell, A.K. Cheetham, D.E. Cox, J.S. Gardner, K. Hanif, A. dos Santos, G.F. Strouse, Phys. Rev. B 61 (2000) 15269–15276.
[8] J.S. Lee, C.C. Kao, C.S. Nelson, H. Jang, K.T. Ko, S.B. Kim, Y.J. Choi, S.W. Cheong, S. Smadici, P. Abbamonte, J.H. Park, Phys. Rev. Lett. 107 (2011) 037206.
[9] H. Kawano, R. Kajimoto, H. Yoshizawa, Y. Tomioka, H. Kuwahara, Y. Tokura, Phys. Rev. Lett. 78 (1997) 4253–4256.
[10] L.S. Ling, S. Tan, L. Pi, Y.H. Zhang, EPL (Europhys. Lett.) 79 (2007) 47008.
[11] J.N. Blandy, A.M. Abakumov, K.E. Christensen, J. Hadermann, P. Adamson, S.J. Cassidy, S. Ramos, D.G. Free, H. Cohen, D.N. Woodruff, A.L. Thompson, S.J. Clarke, APL Mater. 3 (2015) 041520.
[12] S. Jin, X. Chen, J. Guo, M. Lei, J. Lin, J. Xi, W. Wang, W. Wang, Inorg. Chem. 51 (2012) 10185–10192.
[13] E.L. King, H.J. Krall, M.L. Pandow, J. Am. Chem. Soc. 74 (1952) 3492–3496.
[14] S.P. Thompson, J.E. Parker, J. Potter, T.P. Hill, A. Birt, T.M. Cobb, F. Yuan, C.C. Tang, Rev. Sci. Instrum. 80 (2009) 075107.
[15] L.C. Chapon, P. Manuel, P.G. Radaelli, C. Benson, L. Perrott, S. Ansell, N.J. Rhodes, D. Raspino, D. Duxbury, E. Spill, J. Norris, Neutron News 22 (2011) 22–25.
[16] A. Coelho, TOPAS Academic, Version 5, Coelho Software, Brisbane, Australia, 2012.
[17] B.J. Campbell, H.T. Stokes, D.E. Tanner, D.M. Hatch, ISODISPLACE: a web-based tool for exploring structural distortion, J. Appl. Crystallogr. 39 (2006) 607–614.
[18] A.L. Goodwin, M.G. Tucker, M.T. Dove, D.A. Keen, Phys. Rev. Lett. 96 (2006) 047209.
[19] D. Litvin, Magnetic Group Tables: 1-, 2- and 3-Dimensional Magnetic Subperiodic Groups and Magnetic Space Groups, International Union of Crystallography, 2013.
[20] T. Kanashiro, Y. Kishimoto, T. Ohno, Y. Michihiro, Solid State Ion. 40–41 (Part 1) (1990) 308–311.
[21] M. Oliveria, R.K. McMullan, B.J. Wuensch, Solid State Ion. 28–30 (Part 2) (1988) 1332–1337.